

Positron recycling in high energy linear colliders

J. Rossbach

Deutsches Elektronen-Synchrotron, Hamburg, Germany

Received 1 July 1991

A positron recycling scheme is presented which is capable of recovering at least 90% of the disrupted positron beam for a 2×250 GeV linear collider. The beam is separated from the oncoming electron beam and radiation damped in a several kilometers long wiggler section. The beam is then ready to be reinjected into the positron damping ring. Energy spread due to beamstrahlung and beam disruption are considered on the basis of existing numerical as well as analytical studies. Chromatic effects in the separation and matching section are compensated by sextupole magnets. Secondary effects of the wigglers, as for instance transverse emittance growth due to quantum fluctuations and nonlinear field components, are estimated analytically.

1. Introduction

It is a common feature of all high energy electron-positron linear colliders currently under investigation to require a high positron production rate. As seen from table 1, all colliders need an average positron current of the order of 10^{13} s^{-1} . This is to be compared with $7.2 \times 10^{12} \text{ s}^{-1}$ representing the design limit of the present SLC positron source [1]. It is not at all obvious how those high positron currents can be generated. One of the main problems, namely the thermal load within the conversion target, is considerably reduced in the scheme proposed by Balakin and Mikhailichenko using circularly polarized coherent synchrotron radiation from a 300 m long helical undulator

[2]. This scheme, with the additional advantage of producing polarized positrons, is very attractive, but has not been tested so far, because for the undulator radiation photons to exceed the threshold of pair production, the driving electron beam requires more than 100 GeV.

In view of these uncertainties it might be useful to think of a recycling scheme for positrons. The idea presented in this article may be outlined as follows. The positrons are separated from the oncoming electron beam after collision, decelerated in a long wiggler section and reinjected into the positron damping ring. This is schematically shown in fig. 1 together with additional components which are briefly explained in table 2. The main component of the recovery system is

Table 1
Parameters of various linear collider studies

Quantity	CLC	NLC	TLC	JILC	VLEPP	DESY/THD
Energy [GeV]	2×1000	2×250	2×500	2×200	2×1000	2×250
Particles/bunch [$\times 10^9$]	5	16	8	10	100	7
Average rep. rate [Hz]	1690	3600	2200	2000	100	8600
Power/beam [MW]	1.35	2.3	1.4	0.64	1.6	2.4
Inv. emittances x/y [$\times 10^{-6}$ m]	1.5/0.5	6/0.06	2.5/0.025	3/0.03	6/0.06	5/0.05
Rms beam size at IP x/y [nm]	60./12.	560/3.1	190/1	290/2.2	1000/10	173/6
Disruption parameter x/y	0.67/3.3	0.04/7.4	0.033/6.3	0.1/13.4	0.2/20	0.55/15.4
Critical radiation parameter \mathcal{T}_0	1.48	0.43	3.43	0.49	0.60	0.154
Av. fract. energy loss [%]	20	6	19	7.1	20	6
Fractional energy width of disrupted beam (contains 90%) [%]	± 30	± 13	± 25	± 15	± 27	± 11
Av. number of photons	3	1	1.3	1.1	3.2	1
Max. disruption angle x/y [mrad]	0.18/0.19	0.25/0.14	0.18/0.12	0.37/0.13	0.22/0.053	0.36/0.11
Rms bunch length [μm]	200	70	26	60	700	200

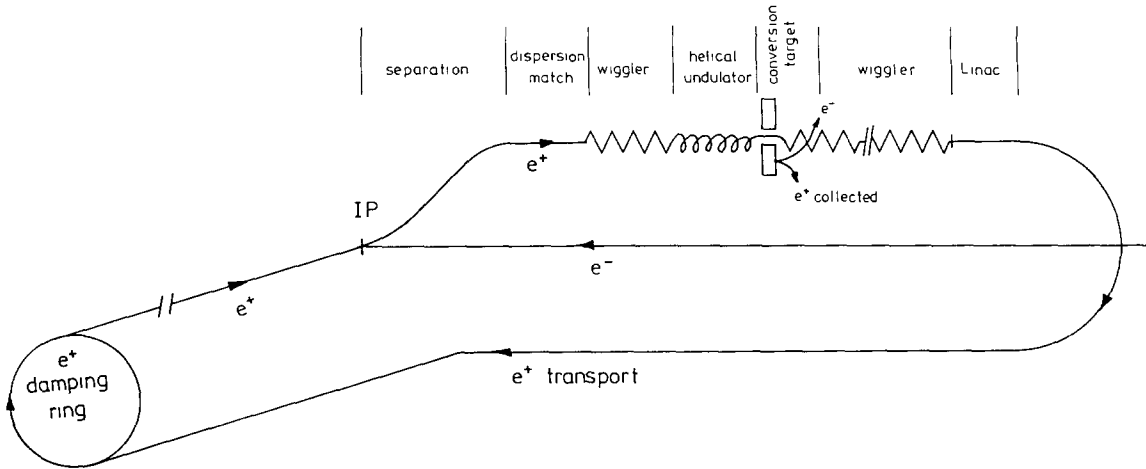


Fig. 1. Sketch of the positron recycling scheme. The helical undulator insertion is not essential for positron recycling but might turn out to be the most elegant way to replace the lost positrons.

the wiggler section of several kilometers length. In this wiggler section, the positrons lose their energy by synchrotron radiation without adiabatic antidamping, i.e. the transverse emittances will remain nearly constant. In addition, a very effective damping of the fractional energy width σ_E/E takes place, which will be very big after collision (of the order of 10%), but small at the end of the wiggler section (less than 1%). Since a very big optical mismatch is tolerable after collision, an energy acceptance of more than $\pm 10\%$ is feasible.

For the DESY/THD linear collider study [3], one expects about 90% recovery efficiency, thus reducing the required positron production rate by a factor of 10. As an additional feature, the helical undulator for pair production might be integrated into the wiggler section as indicated in the sketch of fig. 1. In the second section of this article, the positron beam properties

after collision are discussed. The third section is devoted to the radiation damping in the wiggler section.

2. Positron separation

2.1. Disruption

It is well known that the disrupted beam has to pass the final focus quadrupole magnets of the oncoming beam in order to avoid mechanical damage as well as intolerable high background in the detector. It is very likely that the solution of this problem will require a finite crossing angle of say 1–2 mrad. However, the technical solution sensitively depends on the beam parameters at the interaction point. For the remainder of this section, parameters of the DESY-THD collider

Table 2

Components of the positron recovery system, including a helical undulator for positron replenishment. Instead of the decelerating linac, a synchrotron or a superconducting wiggler may be used alternatively

Distance [m]	Energy [GeV]	Device	Purpose
0–3	250	low β insert	interaction
3–150	250	bending + quadrupole magnets	separation + dispersion match
150–1400	250–100	wiggler	energy damping + deceleration
1400–1700	100	helical undulator	polarized synchrotron radiation for e^+ production
1700–8600	100–7	wiggler	energy damping + deceleration
8600–8800	7–3.15	linac	deceleration
8800–entrance of damping ring	3.15	FODO cells	beam transport
	3.15	storage ring	emittance damping

study are assumed whenever explicit numbers are considered.

In spite of the intense beam–beam forces, the emittance in transverse phase space of positrons is still quite small after collision. The change in emittance is dominated by the disruption angles while the beam diameter remains constant or even decreases due to the pinch effect. The maximum disruption angle $\hat{\theta}$ is estimated by the fit of numerical simulation data [4,5]:

$$\hat{\theta} = 0.9 \frac{D\sigma}{\sigma_x} \left(\frac{1}{1.2 + 50D^3} + \sqrt{0.06 + \frac{D}{3.38}} \right)^{-1}, \quad (1)$$

for round beams, i.e. $\sigma_x = \sigma_y = \sigma$, $D_x = D_y = D$;

$$\hat{\theta}_{x,y} = \frac{2r_e N}{\gamma\sigma_x} k_{x,y} \left[1 + \left(\frac{D_{x,y}}{2} \right)^5 \right]^{-1/6}, \quad (2)$$

for flat beams, with $k_x \approx 0.75$ and $k_y \approx 1.25$.

In these equations, σ_x and σ_y are the horizontal and vertical rms beam sizes at the interaction point (IP) respectively, σ_x is the rms bunch length, $r_e = 2.82 \times 10^{-15}$ m is the classical electron radius, N is the number of particles per bunch in the oncoming beam, γ is the relativistic factor, and D_x and D_y are the parameters of horizontal and vertical disruption, respectively. They are defined by [6]:

$$D_{x,y} = \frac{2r_e N\sigma_x}{\gamma\sigma_{x,y}(\sigma_x + \sigma_y)}. \quad (3)$$

The resulting maximum disruption angles are generally well below 1 mrad (see table 1), representing an increase of angles within the bunch by some factor of ten due to the beam–beam interaction ^{#1}.

With these numbers in mind one can try to find a final focus quadrupole magnet design that allows the disrupted beam to pass. Fig. 2 shows the cross section of one quarter of the DESY/THD linear collider final focus quadrupole. It is a “conventional” iron magnet excited by a single copper conductor [7]. Using a pole tip radius of 0.85 mm it has been shown that the required field gradient of 1300 T/m is attained with tolerable higher order multipole components inside a 0.5 mm aperture radius [8]. If a total crossing angle of 2×0.8 mrad = 1.6 mrad is assumed, the disrupted beam (as well as the beamstrahlung) clears both the final focus lenses while travelling in the area between

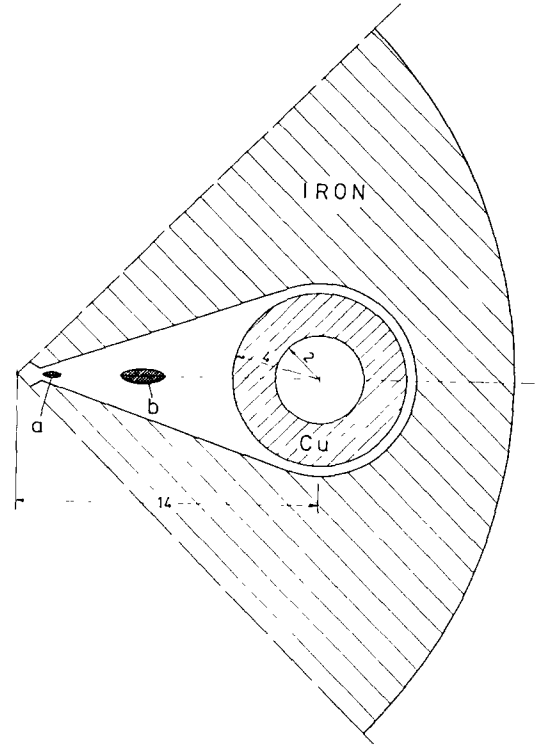


Fig. 2. Cross section of one quarter of the final focus quadrupole of the DESY/THD linear collider study: (a) and (b) are the envelopes of the disrupted beam at the entrance of the first and at the exit of the second final focus lens, respectively. Dimensions are given in mm.

the pure quadrupole field and the copper conductor. In this “window” area the magnetic field of the first (vertically focusing) quadrupole is horizontally focusing as well as horizontally deflecting (with respect to the oncoming beam on the quadrupole axis). This is exactly what one needs for recovery and separation of the disrupted beam. The field strength, however, is comparatively small so that the main part of the job must be done by additional magnets further downstream which act on the disrupted beam alone. Also, the higher order multipole components have not been taken into account yet. They could easily be made tolerable, however, since

- 1) the total field integral is small in this area anyway;
- 2) there is much freedom in designing the shape of the iron pole face in that area.

Fig. 2 contains the envelopes of the disrupted beam at the entrance and at the exit of the final focus doublet. For tracking the beam envelopes, a simple $B_y \sim 1/x$ model has been used for the window area magnetic field, with $B_{y,max} = 1$ T on the pole tips of the first lens and $B_{y,max} = 0.7$ T on the pole tips of the second one.

Fig. 3 shows the trajectories and the envelopes of

^{#1} It should be noted that eqs. (1) and (2) have been derived for head-on collision geometry while some proposals foresee a nonzero crossing angle. With crossing angle, the beam–beam forces cancel out to a considerable extent when integrated over the total interaction (for $D \leq 1$), while for $D \gg 1$ the effect of the crossing angle should be small. I therefore adopt eqs. (1) and (2) as an upper limit for crossing angle geometries.

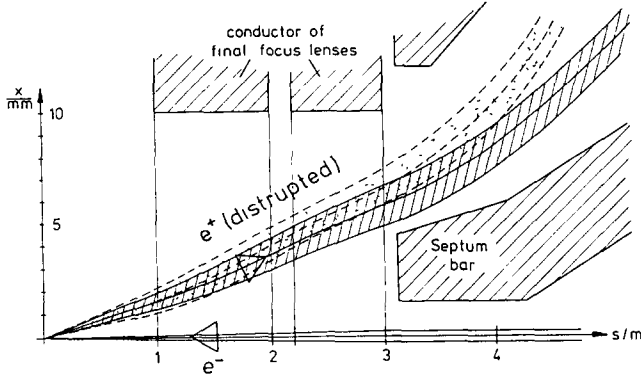


Fig. 3. Envelopes of the disrupted positron beam and the oncoming beam within the final focus doublet and the first part of the septum magnet containing all positrons with energy $> 0.9E_0$. The dotted area marks the envelope of all positrons which have lost 50% of their energy during collision.

the disrupted beam and of the oncoming beam in the horizontal plane.

2.2. Beamstrahlung

The main complication with recovery of positrons, however, is not disruption but the large energy spread due to the beamstrahlung. It is characterized by the critical radiation parameter \mathcal{T} :

$$\mathcal{T} = \frac{2}{3} u_c / E = \lambda_c \gamma^2 / \rho, \quad (4)$$

where E is the particle energy and u_c is the critical beamstrahlung energy due to the characteristic bending radius ρ of the beam-beam force:

$$u_c = \frac{3}{2} \frac{\hbar c \gamma^3}{\rho}, \quad \frac{1}{\rho} \cong \frac{2r_e N}{\gamma \sigma_x (\sigma_x + \sigma_y)}, \quad (5)$$

\hbar is Planck's constant, $\lambda_c = \hbar / m_0 c$ is the Compton wavelength of the electron, and c is the velocity of light.

For the "intermediate" regime $\mathcal{T} \leq 10$ the energy spectrum after collision has been calculated by Yokoya and Chen [9]. It can be expressed approximately by

$$\Psi\left(\frac{E}{E_0}\right) = e^{-N_y} \left[\delta\left(\frac{E}{E_0} - 1\right) + \frac{e^{-y}}{1 - E/E_0} h(y^{1/3} \bar{N}(y)) \right],$$

with

$$y = \frac{1}{\mathcal{T}} - \frac{1}{\mathcal{T}_0}; \quad \mathcal{T}_0 = \mathcal{T}(E_0), \quad (6)$$

$$N_y = \frac{1 - 0.598\mathcal{T}_0 + 1.061\mathcal{T}_0^{5/3}}{1 + 0.922\mathcal{T}_0^2} N_{cl},$$

$$h(x) = \sqrt{\frac{3}{8\pi}} \left(\frac{\sqrt{x/3}}{1 + 0.53x^{-5/6}} \right)^{3/4} \exp\left[4\left(\frac{x}{3}\right)^{3/4}\right],$$

$$\bar{N}(y) = \frac{\mathcal{T}}{\mathcal{T}_0} N_{cl} + \left(1 - \frac{\mathcal{T}}{\mathcal{T}_0}\right) N_y.$$

E_0 is the initial beam energy, and for the average photon number per particle in classical approximation I have adopted [10]

$$N_{cl} = 0.9623 \frac{2\alpha r_e N}{\sigma_x + \sigma_y}, \quad (7)$$

with $\alpha = r_e / \lambda_c \approx 1/137$. The spectra obtained by these semi-empirical formulae fit the numerical simulation results well.

Fig. 4a shows the positron energy spectrum at the end of the entire collision if DESY/THD parameters are used. The spectrum (full line) is normalized as $\int \psi(E/E_0) d(E/E_0) = 1$. The broken line is the integrated probability of fractional energy loss:

$$\eta(E/E_0) = \int_0^{E/E_0} \psi d(E/E_0), \quad (8)$$

i.e. it represents all particles with energy $\leq E$. It is seen that 9% of the particles lose more than 20% of the initial energy. Fig. 4b shows η in linear scale. It is interesting to note that this energy width is determined by $1/\rho^2$ (like ordinary synchrotron radiation power), i.e. by N^2 , see eq. (5). This is illustrated by the broken line in fig. 4b where the number of particles N per bunch was reduced by a factor of 3. For comparison, fig. 5 shows η for CLIC, NLC, TLC and JILC parameters, respectively.

As seen from fig. 4a, the probability of losing more than 50% of the initial energy to beamstrahlung is of the order of 10^{-3} . Since this part of the disrupted beam still contains some 1 kW of beam power, it has to clear the final focus lenses as well. The respective envelope is included in fig. 3 to show that this is indeed the case.

One might argue at first sight that these particles might also suffer twice the maximum disruption angles. For the latter to happen, however, they would have to lose more than 50% of their energy within the first half of the interaction length to suffer increased disruption in the second half. It can already be estimated from fig. 4a that this is extremely improbable. A more precise treatment [9] shows that the probability is in fact of the order of 10^{-9} for DESY/THD parameters, corresponding to 80% energy loss.

2.3. Optics match / mismatch

After passing the final focus lens doublet, the disrupted beam will further be separated from the oncoming beam by a septum magnet, as indicated in fig. 3.

With the magnetic field of $B = 1.5$ T it generates a deflection of 11 mrad within 6 m length plus a gradient of 49 T/m for horizontal focusing. It is pulsed with 50

Hz to shield the oncoming electron beam from stray field by eddy currents in a 5 mm thick septum bar. The stability requirement is of the order of 10^{-3} only. The

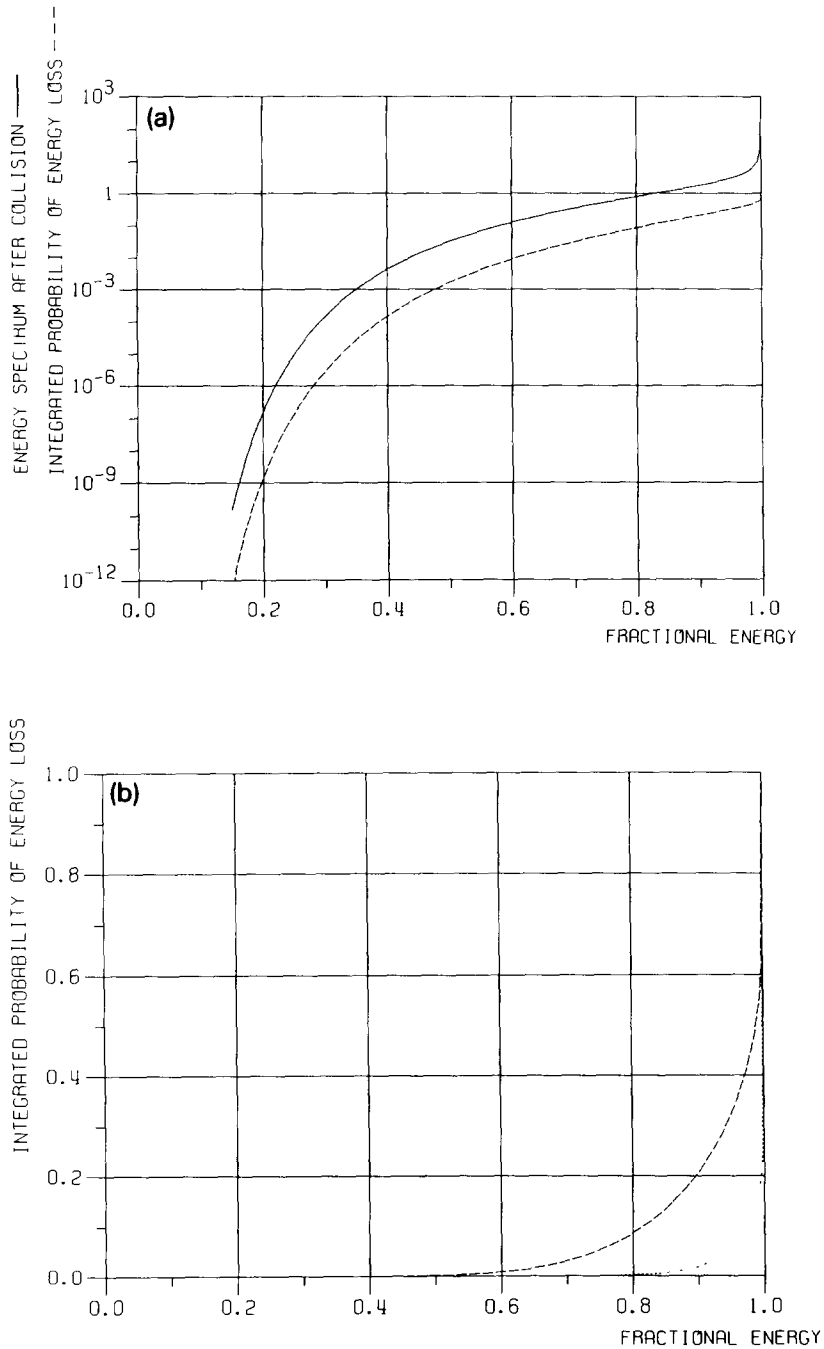


Fig. 4. (a) Energy spectrum ψ after collision (full line) as a function of fractional energy E/E_0 . The dashed line represents the probability η of the fractional energy to be smaller than E/E_0 . DESY/THD linear collider parameters have been adopted (see table 1). An effective beam size of $\sigma_x^{\text{eff}} = 236$ nm has been used to allow for a crossing angle of ± 0.8 mrad. It is seen that 0.1% of the particles lose more than 50% of their initial energy during collision. (b) Probability η in linear scale for the same parameters like in (a) (dashed line) and for 3 times less particles per bunch (dotted line).

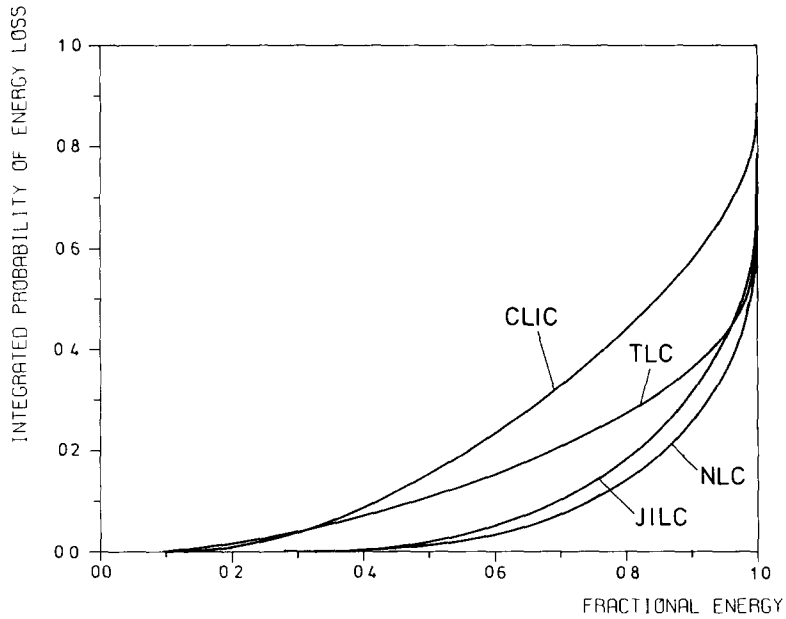


Fig. 5. Probability η of energy loss by beamstrahlung (see eq. (8)) for CLIC, NLC, TLC and JILC parameters, respectively (see table 1).

main purpose of the subsequent optical matching section is:

- 1) to match the recovered positron beam to the periodic solution of the long wiggler magnet section;

- 2) to suppress the dispersion generated by the bending magnets;

- 3) to compensate the chromatic errors of the recovery beamline by sextupole magnets;

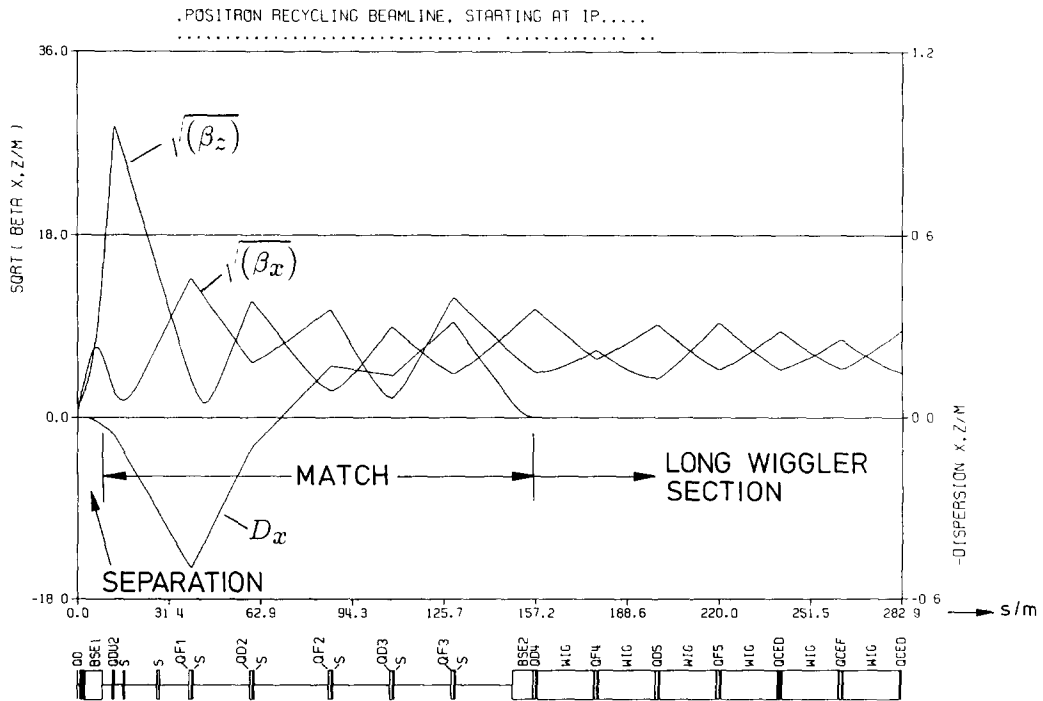


Fig. 6. Linear optics parameters in the first section of the positron recycling beamline for 250 GeV positrons. Labels "S" indicate sextupole positions. The long wiggler section is continued as a periodic FODO lattice.

4) to realign the recovery beamline in parallel with the linac structure of the oncoming beam. This is done by the bending magnet BSE2 at the end of the matching section, see fig. 6. The distance to the linac is from then on about 1.4 m.

As mentioned above, 9% of the positrons lose more than 20% of the initial energy into beamstrahlung (see fig. 4b). The recovery beamline therefore needs some $\pm 10\%$ energy acceptance to achieve a recovery efficiency of 90%. This would be impossible with the recovery optics perfectly matched to the disrupted beam. For the latter, one would have to start the beamline at the collision point with beta function values $\beta_{x,y}^*$ given by

$$\beta_{x,y}^* = \sigma_{x,y} / \hat{\theta}_{x,y}. \tag{9}$$

They are of the order of 10^{-4} m and would necessarily lead to beta values of the order of 10^5 m in the first beamline lenses. This gives huge local chromaticities which, in turn, can be compensated only within a narrow energy bandwidth.

A perfect optical match, however, is not at all necessary. The limiting factor of tolerable mismatch is rather the maximum tolerable emittance $\hat{\epsilon}$ for injection

into the positron damping ring. The damping ring is assumed here to operate at $E_D = 3.15$ GeV with [11]

$$\begin{aligned} \hat{\epsilon}_x &= 4 \times 10^{-6} \pi \text{ m (aperture limit),} \\ \hat{\epsilon}_y &= 2.4 \times 10^{-7} \pi \text{ m (rms beam dimension).} \end{aligned} \tag{10}$$

(The only reason for $\hat{\epsilon}_y$ being so small is that the beam has to attain $\epsilon_y = 6.5 \times 10^{-12} \pi$ m within 5.2 damping times in the DESY/THD design study.) It is essential now, that the long decelerating wiggler section does not increase transverse emittances (as an active linac section would do due to adiabatic antidamping). This is treated in more detail in the next section. We could therefore use the values of eq. (10) for mismatch evaluation if it were not for two minor complications:

- 1) as the efficiency of positron deceleration decreases with γ^2 in the wiggler section, the very last portion of positron deceleration could possibly be done by an active linac (alternatives will be discussed in section 3). The exact energy E_L of takeover is the result of cost minimization. We assume $E_L = 7$ GeV. This reduces the tolerance emittances at the entrance of the wiggler section by a factor of $E_L/E_D \approx 2.2$;
- 2) despite a broad band chromatic correction, some

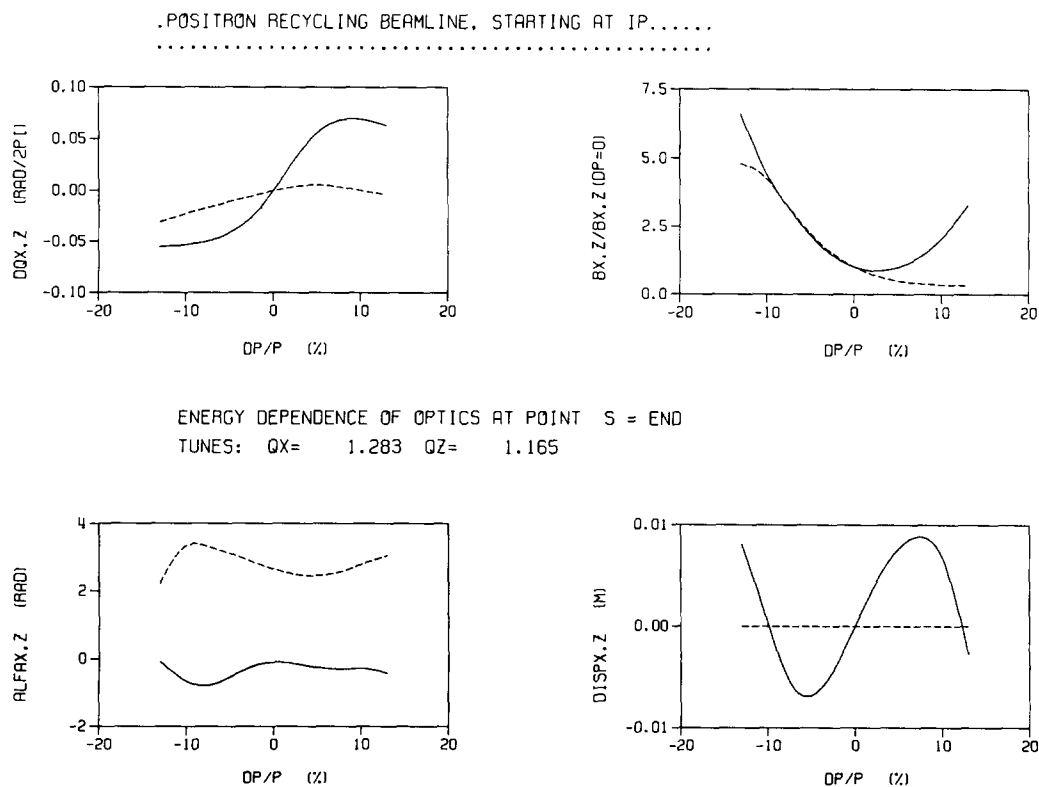


Fig. 7. Energy dependence of linear optics at the end of the matching section.

off-energy beta beat will remain at the end of the matching section. In the present design (which is not very refined yet) it amounts to factors of 6 and 2.5 in the horizontal and vertical plane, respectively (see fig. 7).

With these numbers we can estimate the maximum tolerable emittance values for mismatch at the collision point:

$$\begin{aligned}\tilde{\epsilon}_x &= \frac{1}{2.2} \cdot \frac{1}{6} \cdot 4 \times 10^{-6} \pi \text{ m} = 3 \times 10^{-7} \pi \text{ m}, \\ \tilde{\epsilon}_y &= \frac{1}{2.2} \cdot \frac{1}{2.5} \cdot 2.4 \times 10^7 \pi \text{ m} = 4.4 \times 10^{-8} \pi \text{ m}.\end{aligned}\quad (11)$$

The maximum mismatched beta value is given by

$$\tilde{\beta} = \tilde{\epsilon} / \Theta^2. \quad (12)$$

Since $\tilde{\epsilon}_x$ is derived from the storage ring *acceptance* (i.e. maximum amplitude), it must be related to the *maximum* disruption angle $\hat{\Theta}_x$ (see eq. (2) and table 1)

$$\tilde{\beta}_x = \tilde{\epsilon}_x / \hat{\Theta}_x^2 = 2.3 \text{ m}. \quad (13)$$

$\tilde{\epsilon}_y$, on the other hand, corresponds to rms beam dimensions. Therefore it must be related to the rms disruption angle Θ_y^{rms} , which is smaller than $\hat{\Theta}_y$ by more than a factor of 3 [5,12]:

$$\tilde{\beta}_y = \tilde{\epsilon}_y / (\Theta_y^{\text{rms}})^2 \geq \tilde{\epsilon}_y / \left(\frac{\hat{\Theta}_y}{3}\right)^2 = 32 \text{ m}. \quad (14)$$

The optics shown in fig. 6 uses $\tilde{\beta}_x = 0.3$ and $\tilde{\beta}_y = 2$ m, i.e. there is still a large safety factor. For example, even rms vertical disruption angles 4 times larger than assumed for eq. (14) would be tolerable. In other words, 90% of the disrupted positron beam will end up at the entrance of the damping ring with emittances considerably smaller than required by eq. (10).

The sextupole magnets are arranged in a way which allows both optimum chromatic correction within an energy range of at least $\pm 10\%$ and minimum nonlinear phase space distortion [13]. Fig. 7 shows that the result is quite satisfactory. Chromatic errors of the long wiggler section are negligible since the energy width of the beam is damped very rapidly. The nonlinear phase space distortion on the beam surface is below 20%, i.e. immaterial.

3. Radiation damping

3.1. Radiative deceleration

After the optical matching section the beam enters the main component of the recovery system, a wiggler magnet section several kilometers in length. In this wiggler section the positrons lose their energy by synchrotron radiation. The radiation power is given by [14]

$$P_\gamma = \frac{q^4}{6\pi\epsilon_0 m_0^2 c} B^2 \gamma^2, \quad (15)$$

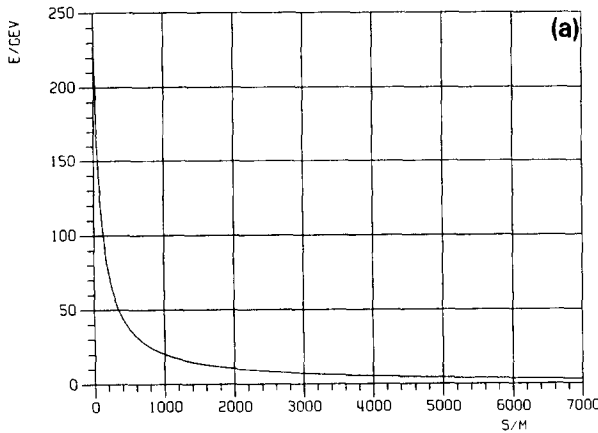
q is the elementary charge, m_0 is the electron rest mass, and ϵ_0 is the dielectric constant of free space. Mks units are used throughout this article.

If s is taken as the longitudinal coordinate, the change of particle energy due to synchrotron radiation is described by

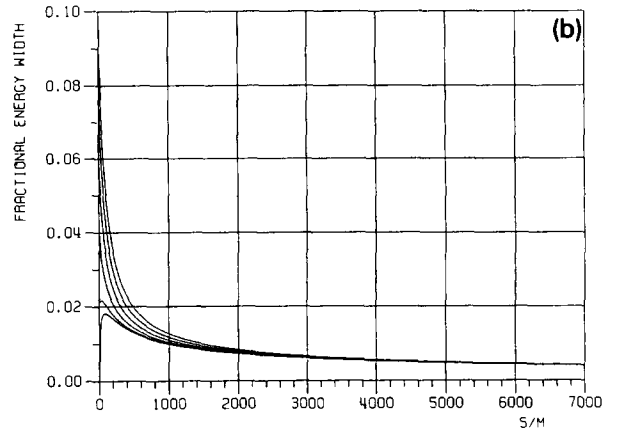
$$\frac{d\gamma(s)}{ds} = -\frac{P_\gamma}{m_0 c^3} = -\Phi B^2 \gamma^2(s), \quad (16)$$

with

$$\Phi = \frac{q^4}{6\pi\epsilon_0 m_0^3 c^4} = 6.466 \times 10^{-10} \text{ m}^{-1} \text{ T}^{-2}.$$



B = 6 TESLA



EO = 250 GEV, B = 6 T

Fig. 8. Evolution of (a) mean particle energy and (b) rms fractional energy width due to radiative deceleration, radiation damping, and quantum fluctuations in a 6 T wiggler field. The final energy is 3.15 GeV. The final energy width $\sigma_\gamma/\gamma = 0.4\%$ is nearly independent of the initial value of $\sigma_{\gamma_0}/\gamma_0$, i.e. it is dominated by quantum fluctuations.

The solution is (with $\gamma_0 = \gamma(s=0)$):

$$\gamma(s) = \frac{E(s)}{m_0 c^2} = \frac{\gamma_0}{1 + \Phi \gamma_0 \int_0^s B^2 d\bar{s}} = \frac{\gamma_0}{1 + \Phi \gamma_0 B_{\text{rms}}^2 s}, \quad (17)$$

$B_{\text{rms}}(s)$ is the rms value of the magnetic field

$$B_{\text{rms}} = \frac{1}{S} \int_0^s B^2 d\bar{s}. \quad (18)$$

As will be shown later on, the period length λ may be quite large (even larger than 1 m). To a good approximation the wiggler magnetic field is therefore assumed to be a piecewise constant dipole field. For the sake of simplicity I use

$$B^2(s) \approx \frac{1}{\lambda} \int_s^{s+\lambda} B^2 d\bar{s} \quad (19)$$

in the remainder of this paper. If $B(s)$ is constant, this means $B^2 = B_{\text{rms}}^2$.

Fig. 8a shows $E(s)$ for superconducting wigglers with $B = 6$ T. While the positrons reach $E = 50$ GeV within a few hundred meters, the remaining 6.5 km are required to arrive at the operation energy of the damping ring (3.15 GeV).

A somewhat more refined version is presented in fig. 9a. As the very high radiation power at high particle energies might be in conflict with superconductor technology, $B = 1.8$ T is assumed within the first 6000 m (e.g. permanent magnet wigglers). Positrons have reached 35 GeV at the end of this section, and the radiation power is only some 500 W/m in the beginning of the subsequent superconducting stage. Also, in order to shorten the expensive superconducting section, it is terminated after 2500 m at $E = 7$ GeV. The final deceleration will be performed by an active linac.

As an alternative to the linac, the positron damping ring might be operated as a decelerating synchrotron [15]. This option offers the additional advantage that adiabatic antidamping of emittances and of energy width are avoided.

The selection of any of these different schemes is mainly a matter of cost minimization.

3.2. Energy damping and quantum fluctuations

Positron recycling is only possible if one finds some mechanism which not only reduces the large spread δE after collision but also the *fractional* energy width $\delta E/E$ while the beam is decelerated. That is, the energy spread must be damped more rapidly than the mean energy.

Radiative energy damping sets in since higher energy particles radiate at more power than lower energy ones, see eq. (15). Let $\gamma(s)$ be the mean particle energy and consider a particle with slightly different energy $\gamma + \delta\gamma$. Eq. (16) yields (using $\delta\gamma \ll \gamma$)

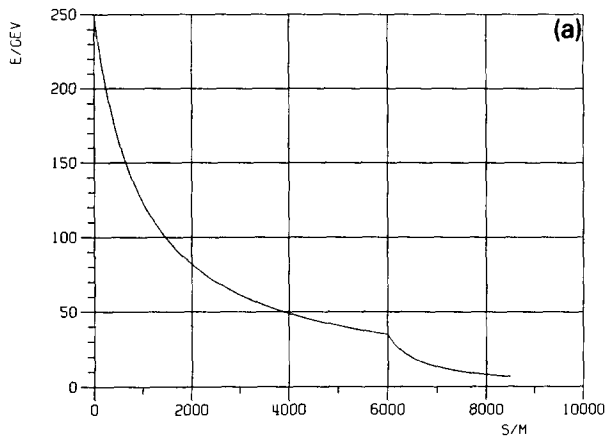
$$\begin{aligned} \frac{d}{ds}(\gamma + \delta\gamma) &= -\Phi B^2(\gamma + \delta\gamma)^2 \\ &\approx -\Phi B^2\gamma^2 - 2\Phi B^2\gamma \delta\gamma, \\ \frac{d}{ds}(\delta\gamma) &= 2\Phi B^2\gamma \delta\gamma. \end{aligned} \quad (20)$$

The solution is (with $\delta\gamma_0$ being the energy error as $s = 0$ and using eq. (17)):

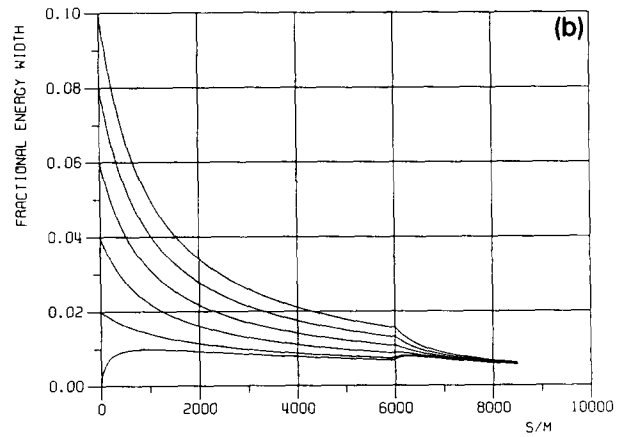
$$\delta\gamma(s) = \delta\gamma_0(1 + \Phi \gamma_0 B^2 s)^{-2} = \delta\gamma_0(\gamma(s)/\gamma_0)^2. \quad (21)$$

It follows that

$$\frac{\delta\gamma(s)}{\gamma(s)} = \frac{\delta\gamma_0}{\gamma_0} \frac{\gamma(s)}{\gamma_0}, \quad (22)$$



$B_1=1.8$ T (6000M), $B_2=6$ T (2500M)



$B_1=1.8$ T (6000M), $B_2=6$ T (2500M), $E=250 \rightarrow 7$ GeV, $DE/E(\text{END}) = 0.006$

Fig. 9. Two-stage scheme with 1.8 T for 6000 m and 6 T for 2500 m. Final energy is 7 GeV. (a) Mean particle energy; (b) rms fractional energy width.

i.e. the fractional energy width decreases in proportion to $\gamma(s)$ (as long as energy fluctuations are neglected)! For statistical reasoning, however, the rate of change of $(\delta\gamma)^2$ is more relevant. It follows from eq. (20):

$$\frac{d}{ds}(\delta\gamma)^2 = 2\delta\gamma \frac{d}{ds}(\delta\gamma) = -4\Phi B^2\gamma(\delta\gamma)^2. \quad (23)$$

Next we have to treat quantum excitation. This will occur as synchrotron radiation is a stochastic process of photon emission. Consequently there is also a competitive excitation of energy fluctuations. The growth rate of the energy variance is given by refs. [16,17] (using the abbreviation $\sigma_\gamma^2 = \langle(\delta\gamma)^2\rangle$).

$$\frac{d}{ds}\sigma_\gamma^2 = \mathcal{N} \frac{\langle u^2 \rangle}{m_0^2 c^5}, \quad (24)$$

\mathcal{N} is the mean rate of synchrotron radiation quanta, and $\langle u^2 \rangle$ is the mean square energy of quanta. It can be expressed by [16]

$$\langle u^2 \rangle = \frac{11}{27}u_c^2, \quad (25)$$

u_c is the critical photon energy

$$u_c = \frac{3}{2}\lambda_c qc\gamma^2 |B|. \quad (26)$$

\mathcal{N} may be expressed by the mean power P_γ (eq. (15)) and the mean quantum energy $\langle u \rangle$:

$$\mathcal{N} = P_\gamma / \langle u \rangle, \quad (27)$$

where [16]

$$\langle u \rangle = \frac{8}{15\sqrt{3}}u_c. \quad (28)$$

Putting all together we get (from now on B means $|B|$)

$$d\sigma_\gamma^2/ds = \Phi\Gamma B^3\gamma^4, \quad (29)$$

with

$$\Gamma = \frac{3}{2} \frac{55}{24\sqrt{3}} \frac{q\lambda_c}{m_0c} \approx 4.5 \times 10^{-10} \text{ T}^{-1}.$$

If we also take averages in eq. (23), we can calculate the gross effect of energy damping and quantum fluctuations:

$$\frac{d}{ds}\sigma_\gamma^2 = \Phi\Gamma B^3\gamma^4 - 4\Phi B^2\gamma\sigma_\gamma^2. \quad (30)$$

The solution of this linear differential equation is

$$\sigma_\gamma^2(s) = e^{-4\Phi\int B^2\gamma ds} \left[\Phi\Gamma \int B^3\gamma^4 e^{-4\Phi\int B^2\gamma ds} ds + \sigma_\gamma^2(s=0) \right]. \quad (31)$$

Ideally, one has to choose $B(s)$ so that $\sigma_\gamma(s=L)$ is minimized at the end of the wiggler section with the additional constraint that B_{rms} yields the required en-

ergy loss, see eq. (17). From this point of view, the magnetic field strength has to decrease with decreasing energy (note that $\sigma_\gamma \propto \gamma^2$, so the damping rate $\propto B^2\gamma^5$, while excitation $\propto B^3\gamma^4$). In practice, however, other considerations are more relevant. The attainable field strength is limited to some 6 T, and even this will be hard to use at high energies because it might be difficult to extract many kilowatts of synchrotron radiation per meter from a superconducting wiggler. For $B(s) = \text{constant}$ we get (using eq. (17))

$$\int B^2\gamma ds = \Phi^{-1} \ln \frac{\gamma_0}{\gamma} \quad (32)$$

and

$$\sigma_\gamma^2(s) = (\gamma(s)/\gamma_0)^4 (\Phi\Gamma B^3\gamma_0^4 s + \sigma_{\gamma_0}^2). \quad (33)$$

Considering again the *fractional* energy width we finally get for its rms value

$$\begin{aligned} \frac{\sigma_\gamma(s)}{\gamma(s)} &= \frac{\gamma(s)}{\gamma_0} \sqrt{\Phi\Gamma B^3\gamma_0^2 s + \left(\frac{\sigma_{\gamma_0}}{\gamma_0}\right)^2} \\ &= \frac{\gamma(s)}{\gamma_0} \sqrt{\Gamma\gamma_0^2 B \left(\frac{1}{\gamma(s)} - \frac{1}{\gamma_0}\right) + \left(\frac{\sigma_{\gamma_0}}{\gamma_0}\right)^2}. \end{aligned} \quad (34)$$

Fig. 8b illustrates the behaviour of σ_γ/γ for different initial energy spread values. They all converge to a comfortably small value of 0.4% at the damping ring energy (3.15 GeV), i.e. the energy spread at the end of the wiggler is dominated by quantum fluctuations. Fig. 9b shows the respective curves for the two stage scheme. Since in this scheme the radiative deceleration is terminated at 7 GeV, the final fractional energy spread will be multiplied by 7/3.15 during linac deceleration. This results in $\sigma_\gamma/\gamma = 1.2\%$ which is still acceptable for the damping ring.

3.3. Transverse emittances

Synchrotron radiation is emitted in the instantaneous forward direction of the individual particle only, within a narrow cone of opening angle $1/\gamma$. Therefore particles lose longitudinal and transverse momentum equally. Consequently transverse emittances will remain constant in the wiggler section. However, this simple picture does not take into account three issues which might nevertheless cause emittance growth, namely:

- 1) If dispersion is generated between the point of quantum emission and the exit of the wiggler section, the energy fluctuations would result in quantum excitation of transverse emittance. According to Sands [16,18], the emittance growth depends on the magnitude of the off-energy dispersion function, η , and its

derivative, η' , at the position of photon emission. This function is identically zero at the beginning of the recovery beamline (i.e. at the IP), and it is matched to zero at the entrance and at the exit of the wiggler section (see fig. 6). In this case, the rate of emittance growth may be estimated at

$$\frac{d\epsilon}{ds} \approx \frac{1}{cE^2} \nu \langle u^2 \rangle \mathcal{N}, \quad (35)$$

with

$$\mathcal{N} = \frac{1}{\beta(s)} \left\{ \eta^2(s) + (\beta(s)\eta'(s) + \alpha(s)\eta(s))^2 \right\}.$$

Using eqs. (15), (25)–(28) this becomes

$$\frac{d\epsilon}{ds} \approx \Gamma \Phi \gamma^2 B^3 \mathcal{N}. \quad (26)$$

Insertion of eq. (17) yields

$$\epsilon(s) \approx \Gamma \Phi \gamma_0^2 \int_0^s \frac{B^3(\bar{s}) \mathcal{N}(\bar{s})}{(1 + \Phi \gamma_0 B^2 \bar{s})^2} d\bar{s} + \epsilon_0. \quad (37)$$

There are two important contributions to $\mathcal{N}(s)$ which I will treat separately.

The first is due to the periodic dispersion which is inevitably generated by the periodic wiggler field. Its contribution to \mathcal{N} is dominated by the term $\beta \eta'^2$ [19] as long as the wiggler period length λ is smaller than some average β in the wiggler (to be explicit I will use $\beta = 100$ m). In a piecewise constant wiggler field the maximum η' will be $\hat{\eta}' = \lambda/(4\rho)$ and thus the mean contribution to \mathcal{N} is

$$\langle \mathcal{N} \rangle_\lambda = \beta \langle \eta'^2 \rangle_\lambda = \frac{\beta}{48} \left(\frac{\lambda}{\rho} \right)^2 = \frac{\beta}{48} \left(\frac{q}{m_0 c} \right)^2 \left(\frac{\lambda B}{\gamma} \right)^2. \quad (38)$$

Eq. (37) now reads

$$\epsilon(s) \approx \Gamma \Phi \frac{\beta}{48} \left(\frac{q}{m_0 c} \right)^2 \int_0^s \lambda^2 B^5 d\bar{s} + \epsilon_0. \quad (39)$$

Since λ and B are at least piecewise constant, the emittance growth in each piece of length L is approximately given by

$$\begin{aligned} \Delta\epsilon &= \epsilon(L) - \epsilon_0 \approx \frac{\Gamma \Phi}{48} \left(\frac{q}{m_0 c} \right)^2 \beta \lambda^2 B^5 L \\ &\approx \frac{2.1 \times 10^{-15}}{m^3 T^5} \beta \lambda^2 B^5 L. \end{aligned} \quad (40)$$

Since we assume plane horizontal wigglers, this growth takes place in the horizontal plane only. If we compare with $\hat{\epsilon}_x$ from eq. (10), we find that the emittance growth due to the intrinsically generated dispersion is

negligible as long as $\Delta\epsilon_x \ll 4 \times 10^{-6} \pi$ m. For the (worst) case of $B = 6$ T, $L = 7000$ m this requires

$$\lambda^2 \ll 0.35 \text{ m}^2,$$

which is easy to fulfil.

The second contribution to $\mathcal{N}(s)$ which has to be considered is due to orbit errors and quadrupole misalignments. This can only be taken into account on a statistical basis. As a rough estimate it suffices to replace $\mathcal{N}(s)$ by some average value $\langle \mathcal{N} \rangle_{\text{dist}}$ (note that strictly speaking \mathcal{N} must be weighted more at high energies). If we further assume $|B(s)| = \text{const.}$, we may integrate eq. (37) obtaining

$$\epsilon(s) \approx \Gamma \Phi \gamma_0^2 B^3 \langle \mathcal{N} \rangle_{\text{dist}} \frac{s}{1 + \Phi \gamma_0 B^2 s} + \epsilon_0. \quad (41)$$

For $s \gg (\Phi \gamma_0 B^2)^{-1}$ this converges to

$$\epsilon_\infty \approx \Gamma \gamma_0 B \langle \mathcal{N} \rangle_{\text{dist}} + \epsilon_0. \quad (42)$$

As this effect may occur horizontally as well as vertically, we now have to compare $\epsilon_\infty - \epsilon_0$ with $\hat{\epsilon}_x$ and $\hat{\epsilon}_y$ from eq. (10), respectively. For this contribution to remain negligible it is necessary that

$$\langle \mathcal{N} \rangle_{\text{dist},x} \ll 0.002 \text{ m}, \quad \langle \mathcal{N} \rangle_{\text{dist},y} \ll 0.0001 \text{ m}. \quad (43)$$

These values correspond to spurious dispersion function amplitudes of

$$\hat{\eta}_{\text{dist},x} \ll 0.4 \text{ m}, \quad \hat{\eta}_{\text{dist},y} \ll 0.1 \text{ m}, \quad (44)$$

which do not represent impracticable tolerance requirements.

2) It has been stated before that the synchrotron radiation quanta are emitted within a narrow cone of opening angle $1/\gamma$. This means that there are also some quanta which deflect the particle at the instant of emission. The following crude estimation shows that this effect is negligible:

Let all quanta have energy u_c (in fact those with lower energy are emitted into a somewhat larger cone, but their contribution to angular diffusion would be smaller nevertheless). The rms deflection angle σ_φ of the electron after the emission of one quantum is then

$$\begin{aligned} \sigma_{\varphi,1} &\approx \frac{1}{\gamma} \times \text{photon momentum/electron momentum} \\ &= \frac{1}{\gamma} \frac{u_c}{E} \end{aligned}$$

Note that this quantity is independent of γ if B is fixed.

Since quanta are emitted at a rate \mathcal{N} (eq. (27)), the rms angle after a distance L will be

$$\sigma_\varphi(L) \approx \sqrt{\mathcal{N} \frac{L}{c} \frac{u_c}{\gamma E}}. \quad (45)$$

This generates an emittance of

$$\Delta\epsilon(L) \approx \beta\sigma_\phi^2 = \beta \frac{P_y}{u_c} \frac{Lu_c^2}{c\gamma^2 m_0^2 c^4 \gamma^2} \approx \Phi\Gamma\beta B^3 L. \quad (46)$$

This is for any reasonable B several orders of magnitude smaller than the tolerable emittances.

3) Even a perfect wiggler contains nonlinear field contributions due to the alternation of the field direction [20]. This induces phase space filamentation and eventually some growth of the effective emittance. The nonlinear kick on the particle trajectory per wiggler period λ may be estimated at [21]

$$\begin{aligned} \Delta y'_\lambda(s) &= \frac{1}{3\lambda} \left(\frac{2\pi}{\rho(s)} \right)^2 y^3 \\ &= \frac{1}{3\lambda} \left(\frac{2\pi q}{m_0 c} \right)^2 (\epsilon_y \beta_y)^{3/2} \left(\frac{B}{\gamma(s)} \right)^2. \end{aligned} \quad (47)$$

It depends on the vertical beam size and vanishes for a perfectly aligned absolutely flat beam. The contributions of successive periods accumulate coherently between successive quadrupole lenses, i.e. within distances l_q of say 50 m, otherwise they accumulate more or less incoherently (except for resonances which are assumed to be avoidable). The cumulated squared nonlinear kick per distance L is therefore

$$(\Delta y')^2 = \int_0^L \frac{ds}{l_q} \frac{l_q^2}{\lambda^2} (\Delta y'_\lambda(s))^2. \quad (48)$$

Using eqs. (47) and (17) the effective emittance growth due to this nonlinear kick is finally estimated at (in the limit $L \gg (\Phi\gamma_0 B^2)^{-1}$):

$$\Delta\epsilon_y(L) \approx \beta_y (\Delta y')^2 \approx \frac{1}{45} \left(\frac{2\pi q \Phi}{m_0 c} \right)^4 \frac{l_q B^{12} L^5}{\lambda^4} \epsilon_y^3 \beta_y^4, \quad (49)$$

ϵ_y is the vertical emittance of the disrupted beam in the wiggler section, i.e. including not only disruption but also on-energy as well as off-energy mismatch. From sections 2.1 and 2.2 I expect $\epsilon_y \approx 3 \times 10^{-9} \pi$ m. Using $l_q = 50$ m, $B = 6$ T, $L = 7000$ m, $\lambda = 0.3$ m and $\beta_y \approx 100$ m we get

$$\Delta\epsilon_y \approx 4 \times 10^{-10} \pi \text{ m.}$$

These considerations show that the nonlinear field components in the wigglers are tolerable but by no means negligible. Although "worst case" parameters have been used in the estimations, the situation might nevertheless be even worse in reality because of the fabrication tolerances of wigglers etc. More detailed studies are required to deal with these questions.

Acknowledgements

I am indebted to R. Brinkmann, J. Pflüger and G.A. Voss for valuable discussions and to S. Wipf for carefully reading the manuscript.

References

- [1] B. Richter, Part. Accel. 26 (1990) 33; thus far this source is reported to yield $3.8 \times 10^{10} \text{ s}^{-1}$ per pulse at 60 Hz with no problem turning up the repetition rate to 120 Hz.
- [2] V.E. Balakin and A.A. Mikhailichenko, Proc. 12th Int. Conf. on High Energy Accelerators, Fermilab, Chicago, 1983, eds. F.T. Cole and R. Donaldson.
- [3] DESY/TH-Darmstadt Linear Collider Study Group, Design Study of a 500 GeV Linear Collider, Proc. 1990 Linear Accelerator Conf., Albuquerque, NM, Sept. 1990 (Nat. Techn. Inform. Service, US Dept. of Commerce, Springfield, VA 22161, 1990).
- [4] A. Minten, Disruption angles, SLAC-CN-305 (1985).
- [5] R.B. Palmer, Prospects for high energy e^+e^- linear colliders, SLAC-PUB-5195 (1990).
- [6] R. Hollebeek, Nucl. Instr. and Meth. 184 (1981) 333.
- [7] H. Wuempelmann, private communication.
- [8] Ch. McDowell, Field calculation and optimization of a linear collider final focus quadrupole lens with tri-planar pole tips, DESY M-90-10 (1990).
- [9] K. Yokoya and P. Chen, Electron energy spectrum and maximum disruption angle under multi-photon beamstrahlung, SLAC-PUB-4935 (1989).
- [10] K. Yokoya, Nucl. Instr. Meth. A251 (1986) 1.
- [11] R. Brinkmann, A study of low-emittance damping ring lattices, DESY M-90-09 (1990).
- [12] P. Chen, An Introduction to Beamstrahlung and Disruption, Lecture Notes in Physics 296 (Springer, 1988).
- [13] The sextupole optimization as well as optics graphics are performed by R. Brinkmann's extension of the COMFORT program.
- [14] J.-D. Jackson, Classical Electrodynamics (Wiley, 1975).
- [15] The idea to use a decelerating synchrotron is due to R. Brinkmann.
- [16] M. Sands, The Physics of Electron Storage Rings, An introduction, SLAC-121 (1970).
- [17] J.M. Jowett, Introductory statistical mechanics for electron storage rings, AIP Conf. Proc. 153 (1987).
- [18] M. Sands, Emittance growth from radiation fluctuations, SLAC/AP-47 (1985).
- [19] N.S. Dikanskii and A.A. Mikhailichenko, Straightline cooling system for obtaining high energy beams e^+ , e^- with minimal emittance, INP Preprint 88-9 (1988).
- [20] K. Halbach, Nucl. Instr. and Meth. 187 (1981) 109.
- [21] P. Kuske and J. Bahrdt, Influence of the BESSY undulator on the beam dynamics, Proc. EPAC, Nice, 1990 (Ed. Frontières, 1990).